Since January 2020 Elsevier has created a COVID-19 resource centre with free information in English and Mandarin on the novel coronavirus COVID-19. The COVID-19 resource centre is hosted on Elsevier Connect, the company's public news and information website.

Cytokine 125 (2020) 154833

Contents lists available at ScienceDirect

Cytokine

journal homepage: www.elsevier.com/locate/cytokine

Structure-based glycoengineering of interferon lambda 4 enhances its productivity and anti-viral potency

Jae-Hee Chung[a,1], Seon-Hui Hong[b,1], Nari Seo[c], Tae-Shin Kim[d], Hyun Joo An[c], Pedro Lee[d], Eui-Cheol Shin[b,d,*], Ho Min Kim[b,d,e,*]

[a] Department of Biological Sciences, Korea Advanced Institute of Science and Technology (KAIST), 291 Daehak-ro, Yuseong-gu, Daejeon 34141, Republic of Korea
[b] Biomedical Science and Engineering Interdisciplinary Program, Korea Advanced Institute of Science and Technology (KAIST), 291 Daehak-ro, Yuseong-gu, Daejeon 34141, Republic of Korea
[c] Graduate School of Analytical Science & Technology, Chungnam National University, Daejeon 34134, Republic of Korea
[d] Graduate School of Medical Science & Engineering, Korea Advanced Institute of Science and Technology (KAIST), 291 Daehak-ro, Yuseong-gu, Daejeon 34141, Republic of Korea
[e] Center for Biomolecular & Cellular Structure, Institute for Basic Science (IBS), Daejeon 34126, Republic of Korea

ARTICLE INFO

Keywords:
IFNλ4
Glycoengineering
Homology modeling
Type III interferon signaling
Anti-viral activity

ABSTRACT

Interferon lambda 4 (IFNλ4) has been recently known and studied for its role in hepatitis C virus (HCV) infection, but its clinical potential is significantly hampered due to its poor expression *in vitro*. Our study reports the successful production of IFNλ4 from a mammalian cell line through a glycoengineering and structure-based approach. We introduced *de novo* N-glycosylation of IFNλ4, guided by structural analysis, and produced IFNλ4 variants in Expi293F that displayed improved expression and potency. To preserve the structure and functionality of IFNλ4, the model structure of the IFNλ4 signaling complex was analyzed and the N-glycosylation candidate sites were selected. The receptor binding activity of engineered IFNλ4 variants and their receptor-mediated signaling pathway were similar to the E. coli version of IFNλ4 (eIFNλ4), while the antiviral activity and induction levels of interferon-stimulated gene (ISG) were all more robust in our variants. Our engineered IFNλ4 variants may be further developed for clinical applications and utilized in basic research to decipher the immunological roles of IFNλ4.

1. Introduction

Interferons (IFNs) are a group of cytokines that serve as the first line of defense against viruses. In addition to their protective role against viral infection, the interferon (IFN) family - consisting of types I, II, and III IFNs, have numerous additional functions that influence cellular growth and immune surveillance against tumor cells [1–3]. All three IFN members activate the JAK/STAT pathway and induce interferon-stimulated gene (ISG) expression by binding to their respective receptors: IFNαR1 and IFNαR2 for type I interferon (IFNα/β), IFNγR1 and IFNγR2 for type II interferon (IFNγ), and IFNλR1 and IL10Rβ for type III interferon (IFNλ1∼4) [1,4]. In contrast to types I and II, type III IFN was only recently identified and plays not only antiviral functions but also novel immunomodulatory functions in oncology and autoimmune diseases [5,6]. IFNλ1∼3 were identified through computational based prediction from genome sequencing [7,8] and IFNλ4 was discovered in genome-wide association studies (GWAS) on hepatitis C virus (HCV)-infected patients [9]. The ΔG allele of a dinucleotide genetic variant (rs368234815) that is upstream of the IFNL3 locus on chromosome 19 creates the functional IFNλ4, while the TT allele leads to a frameshift, thereby rendering it a pseudogene [9]. Interestingly, HCV patients with the ΔG allele and hence expressing IFNλ4, responded poorly to PEGylated-IFNα-ribavirin treatment as compared to patients with the TT allele [10]. However, IFNλ4 still induces the major hepatic ISG expression during chronic HCV infection and is able to drive the anti-viral response against other viruses such as the MERS-CoV *in vitro* [11]. Similar to IFNα (Roferon-A for hairy cell leukemia) and IFNβ (Avonex for multiple sclerosis), successful phase 2 clinical trials of PEGylated IFNλ1 against hepatitis D virus (HDV) infection highlight the pharmaceutical potential of the IFNλ family.

Previously, the transient expression of wild-type IFNλ4 in mammalian cells failed to produce significant amounts of recombinant

* Corresponding authors at: Graduate School of Medical Science & Engineering, KAIST, 291 Daehakro, Yuseong-gu, Daejeon 34141, Republic of Korea.
E-mail addresses: ecshin@kaist.ac.kr (E.-C. Shin), hm_kim@kaist.ac.kr (H.M. Kim).
[1] These authors contributed equally to this work.

https://doi.org/10.1016/j.cyto.2019.154833
Received 7 May 2019; Received in revised form 21 August 2019; Accepted 27 August 2019
Available online 31 August 2019

IFNλ4. It was suggested that a weak signal peptide in IFNλ4 may be responsible for its impaired secretion and that proper glycosylation of IFNλ4 may be required for its secretion [9]. Although recombinant IFNλ4 can be purified from a bacterial expression system through refolding the inclusion body [11], a lack of glycosylation may affect the efficacy of IFNλ4. Recently, glyco-engineering, which introduces new glycosylation sites or alters the glycan composition of CHO cells, has been widely used to produce improved therapeutic proteins, because glycan moieties can affect various protein properties, such as solubility, stability, *in vivo* activity, and serum half-life. For example, improved half-life and productivity are obtained from glyco-engineered hIFNβ-1a and hIFNα [12,13]. Moreover, increased secretion of lipase, cutinase, llama V_{HH} antibody, and macrophage inhibitory cytokine 1 results from the addition of a single N-glycosylation site [14,15]. Therefore, we propose that glyco-engineering IFNλ4 is a viable option for improving its expression level and possibly altering other properties.

In this study, we used mutagenesis to introduce new potential N-glycosylation sites based on the model structures of the IL10Rβ-IFNλ4-IFNλR1 complex. Our results indicate that, among several IFNλ4 variants, three - L28N, P73N, and L28N + P73N - exhibited enhanced productivity, although only P73N was glycosylated *de novo*. Moreover, these HEK293-expressed IFNλ4 variants retained their binding affinity to the specific IL10Rβ and IFNλR1 receptors, and showed a more potent IFNλ4-mediated signaling and antiviral activity than did *E. coli*-derived IFNλ4 (eIFNλ4).

2. Materials and methods

2.1. Modeling process

The human IFNλ4 amino acid sequence (22~179, NCBI Accession Number: AFQ38559.1) was used in SWISS-MODEL homology modeling with three templates (PDB code: 5T5W.1.C, 3OG6.1.A, 3OG4.1.A). The model with the highest QMEAN-Z (Qualitative Model Energy ANalysis-Z) score (−2.56) was aligned to the IL10Rβ-IFNλ3-IFNλR1 structure (PDB code: 5T5W) to create the IL10Rβ-IFNλ4-IFNλR1 model.

2.2. Cell lines, cell culture, and reagents

Expi293F (#A14527, Gibco®) cells were cultured according to ATCC guidelines and used within 6 months of receipt. They were maintained in suspension in Expi293F expression medium (#14351, Gibco®) at 37 °C and 8% CO_2 with 125 rpm agitation. Huh-7.5 cells (Apath) were maintained at 37 °C with 5% CO_2 in Dulbecco's modified Eagle medium (DMEM) containing 10% fetal bovine serum (WelGENE), 4.5 g/l glucose, L-glutamine, and 1% penicillin/streptomycin (WelGENE). Small-interfering RNAs (siRNAs) against IFNλR1 and scrambled sequences were obtained from Santa Cruz Biotechnology. Transfection of IFNλR1 siRNA was performed using lipofectamine RNAi MAX (Invitrogen). Recombinant IFN-α-2a was obtained from PBL Assay Science, recombinant IFN-β was obtained from PeproTech, and recombinant human IFNλ1 (1598-IL), λ2 (8417-IL), λ3 (5259-IL), and eIFNλ4 (9165-IL) were obtained from R&D Systems.

2.3. Expression and purification of recombinant proteins

Gene encoding human IFNλ4 (1~179) was cloned into a modified pcDNA3.1 (#V79020, Invitrogen™) containing a C-terminal 6x-His tag. IFNλ4 variants were generated by site-directed mutagenesis (QuikChange site-Directed Mutagenesis Kit, #200519, Agilent) using the IFNλ4 wild-type construct as the PCR template. The primers for site-directed mutagenesis are listed in Supplementary Table 1. For IFNλ4-Protein A expression, the C-terminal 6x-His in the IFNλ4 constructs were replaced with a Protein A gene derived from PEZZ18 (#VPT4033, GE Healthcare life Sciences). A thrombin cleavage sequence (LVPRGS) was introduced between the IFNλ4 genes and the Protein A gene using the PCR primer, in order to remove Protein A. IFNλ4 wild-type and variants containing 6x-His or Protein A were transfected into Expi293F cells using ExpiFectamine 293 Transfection Kits (#A14524, Invitrogen™), following the manufacturer's protocol. For the purification of IFNλ4 variants, the supernatant containing secreted IFNλ4-Protein A was loaded onto IgG Sepharose resin (#17096902, GE Healthcare Life Sciences). After three washes with 1x PBS, the protein-bound resins were incubated overnight with thrombin (1% (v/v) in 1x PBS) at 4 °C to remove the C-terminal Protein A tag. Eluted IFNλ4 variants were subsequently purified by gel-filtration chromatography in a Superdex 200 Increase 10/300 GL column (#28990944, GE Healthcare Life Sciences) equilibrated with 1x PBS.

2.4. Immunoblotting

The cells were lysed with RIPA buffer (Thermo Fisher Scientific) to prepare total cell lysates. Ten micrograms of each cell lysate were loaded on SDS-PAGE gels prior to immunoblotting. The antibodies used for immunoblotting were: IFNλ4 (1:200, mouse, Millipore MABF227), IFNλ4 (1:200, rabbit, Abcam ab196984), STAT1 (1:1000, rabbit, BD Biosciences 610120), PY-STAT1 (1:1000, mouse, BD Biosciences 612233), STAT2 (1:1000, rabbit, Santa Cruz Biotechnology sc-476), IRF9 (1:1000, rabbit, Santa Cruz sc-496), SOCS1 (Abcam #62584), USP18 (Cell Signaling Technology #4813), horseradish peroxidase (HRP)-conjugated rabbit IgG (1:5000, Abcam ab97051), and HRP-conjugated mouse IgG (1:5000, Abcam ab97023).

2.5. PNGase F treatment

N-glycans of IFNλ4 were removed using a PNGase F kit (#P0704S, New England Biolabs) according to the manufacturer's instructions. Briefly, IFNλ4 variants were boiled with Glycoprotein Denaturing Buffer (10×) and chilled on ice. GlycoBuffer(10×), NP-40(10×), and 1 μl of PNGase F were added onto denatured proteins and the mixture was incubated at 37 °C for 1 h before the Western blot analysis.

2.6. Glycosylation site analysis

The glycopeptides resulting from non-specific digestion were prepared as previously described [16]. Briefly, 50 μg/μL IFNλ4 variants were incubated with 50 μg/μL pronase E for 1 h at 37 °C. The digested glycopeptides were enriched by graphitized carbon solid-phase extraction (PGC-SPE) and analyzed by nanoLC-Chip Q-TOF MS (Agilent Technologies). The LC-MS and MS/MS data were processed and interpreted as previously described, using MassHunter Qualitative Analysis software (version B.07.00, Agilent Technologies) and GP Finder software [17].

2.7. Determination of binding kinetics

The IFNλ4 variant binding kinetics to IFNλR1 and IL10Rβ were measured by biolayer light interferometry on a BLItz system (ForteBio, Pall Life Sciences). The mixtures were agitated at 2200 rpm in washing buffer (200 mM NaCl, 20 mM Tris-HCl pH 8, 5% glycerol, 0.01% Tween-20). Assays were performed at room temperature. Biotinylated IFNλ4, at concentrations of 0.25 mg/ml, were loaded onto the surfaces of streptavidin biosensors (ForteBio) for 1 min, followed by washing of the loaded biosensors for 2 min with washing buffer (200 mM NaCl, 20 mM Tris-HCl pH 8, 5% glycerol, 0.01% Tween-20) to remove any unbound protein. The biosensor tips were immersed in drops containing indicated concentration of IFNλR1 and IL10Rβ (500, 1000 and 2000 nM). Associations (on rate, k_{on}) were measured over a 2 min interval. The sensors were subsequently immersed in washing buffer for 2 min to measure dissociation (off-rate, k_{off}). K_D, measured in nanomoles, was calculated as the ratio of off-rate to on-rate. The resulting data were analyzed by fitting to a 1:1 ligand model with the global

fitting function.

2.8. Production and infection of cell culture-derived HCV (HCVcc)

The Japanese fulminant hepatits-1 (JFH-1) strain (genotype 2a) of HCVcc was produced as described previously [18]. DMEM containing 5% human serum was used to culture the Huh-7.5 cells, in order to produce highly infectious JFH1 HCVcc. HCVcc infectivity was quantified by a colorimetric focus-forming assay, as described previously [19]. Huh-7.5 cells were infected with JFH-1 HCVcc at 0.5 multiplicity of infection (MOI).

2.9. RNA extraction and real-time quantitative PCR

Total RNA isolation and TaqMan real-time quantitative PCR were performed as described previously [20]. In brief, total RNA was isolated with GeneAll Ribospin™ (GeneAll), after which TaqMan Gene Expression Assays (Applied Biosystems) were used to determine the mRNA levels of the target genes. Quantification of intracellular HCV RNA copies was performed as described previously [20]. The results were standardized to the mRNA levels of GAPDH and the data are presented as means ± standard error of the mean. TaqMan Assay (Applied Biosystems) used in this study are: IFNLR1 (Hs00417120_m1), ISG15 (Hs01921425_s1), MX1 (Hs00895608_m1), SOCS1 (Hs00705164_s1), USP18 (Hs00276441_m1), GAPDH (Hs02758991_g1). IFNL proteins (R &D Systems) used in this study are: IFNL1 (1598-IL), IFNL2 (8417-IL), IFNL3 (5259-IL), eIFNL4 (9165-IL).

2.10. Statistical analysis

Data from experiments with cell lines are presented as means ± standard error of the mean. Unpaired *t*-tests or two-tailed Mann-Whitney U-tests were performed for statistical analysis. All of the analyses for real-time quantitative PCR were performed with GraphPad Prism version 7.01. P values less than 0.05 were considered to be statistically significant.

3. Results

3.1. Design and expression of IFNλ4 variants

The low affinity of wild-type IFNλ to its receptor, IL10Rβ, hampers the production of the stable ternary complex - IL10Rβ-IFNλ-IFNλR1. Therefore, only the structures of IFNλ3 alone [21] or IFNλ1 in complex with IFNλR1 [22] have been determined. Recently, Mendoza, *et al.*, introduced affinity-enhancing mutations on IFNλ3 which stabilized its interaction with IL10Rβ, and elucidated the crystal structure of the type III interferon signaling complex, IL10Rβ-IFNλ3-IFNλR1 (PDB code: 5T5W) (Fig. 1A) [23]. Although IFNλ4 shares only ~30% sequence identity with IFNλ1~3, the sequence alignment of IFNλ1~4 suggests that IFNλ4 interacts with IFNλR1 and IL10Rβ in a similar manner as the IL10Rβ-IFNλ3-IFNλR1 ternary complex [23] for two reasons. First, the amino acids of the IFNλ family that are critical for IFNλR1 binding are well-conserved in IFNλ4 (P37, L40, K44, R47, D48, I108, F159, and R163) (Fig. 1B). Second, hydroxyl groups of several aromatic residues of IL10Rβ (Y59, Y82, Y140, and W143) form a hydrogen bonding network with IFNλ3 (S44, L45, Q48R, and E106D); these are also well conserved in IFNλ4 (S34, L35, R48, and Q100). Therefore, we modeled the IFNλ4 structure using the crystal structure of IFNλ3 and IFNλ1 (Fig. 1A) and structurally aligned it to the IL10Rβ-IFNλ3-IFNλR1 structure to build the IL10Rβ-IFNλ4-IFNλR1 model (Fig. 1B). Interestingly, the model structure of IL10Rβ-IFNλ4-IFNλR1 indicates that critical hydrophobic pockets for harboring the hydrophobic residues of IL10Rβ (Y82 and W143) are well maintained on the surface of IFNλ4 (Fig. 1C).

Using the IL10Rβ-IFNλ4-IFNλR1 model structure, we searched the new N-glycosylation candidate sites of IFNλ4 based on three criteria. First, the sites had to be outside the receptor binding region to minimize the change in the receptor-ligand binding and signal activation. Second, they had to be exposed to the solvent to allow access to oligosaccharyltransferase (OST), which catalyzes the initial transfer of glycan from the lipid-linked oligosaccharide onto the substrate asparagine [24,25]. Third, the consensus sequence (NXS/T, X = any amino acid except proline) had to be achieved by single point mutation to minimize the structural distortion caused by the mutation. Only six candidate sites were available that met all three criteria: L28N, A54N, P73N, H97N, K154N, and A173N (Fig. 1A and B). We named them M1 ~ M6, respectively.

Next, we examined the expression levels of each of the IFNλ4 variants (M1 ~ M6) by western blot and found that two IFNλ4 variants, M1 (L28N mutation) and M3 (P73N mutation), resulted in enhanced protein expression (Fig. 2A). Interestingly, only M3 showed the prominent up-shift in SDS-PAGE that indicates successful hyperglycosylation. We also checked the expression level of the double mutants (L28N and P73N, M7), showing further enhanced protein expression compared to M1 and M3 variants (Fig. 2A). The constructs used in the western blot for hit discovery carried a C-terminus 6x Histidine tag, which may interfere with proper secretion of the protein, given the extensive distribution of positively-charged amino acids in IFNλ4. Therefore, we substituted the 6x histidine tag with a protein A tag and purified three IFNλ4 variants (M1, M3, and M7) using affinity chromatography followed by thrombin digestion, in order to remove the protein A tag and subsequent size exclusion chromatography. Final IFNλ4 variants (M1, M3, and M7) were analyzed by SDS-PAGE and Coomassie blue staining under reducing and non-reducing condition. The resulting bands indicate that three IFNλ4 variants (M1, M3, and M7) are monomer (Fig. 2B). The elution profile of standard proteins indicates that each monodispersed peak corresponds to the IFNλ4 variants (~44 kDa) (Fig. 2C). Most likely, this oversized elution is due to the presence of N-glycosylation on IFNλ4 variants, which was confirmed by the results shown in the following section.

3.2. Identification of N-glycans on IFNλ4 variants

To identify the presence of N-glycans on the three IFNλ4 variants, we treated them with PNGase F and compared their sizes with SDS-PAGE. The M3 (P73N) and M7 (L28N + P73N) IFNλ4 variants were located at higher molecular weight positions compared to the M1 (L28N) IFNλ4 variant. After de-glycosylation with PNGase F, however, the molecular weight of the three IFNλ4 variants decreased to the same level, indicating the presence of N-glycans in all IFNλ4 variants, but the status or position of M1 N-glycosylation may be slightly different from those of M3 and M7 IFNλ4 variants (Fig. 3A).

We used mass spectrometry to determine the exact position of N-glycans on IFNλ4 variants [26]. Briefly, purified IFNλ4 variants were treated with pronase E to produce glycopeptides, and ultimately to determine the glycosylation site. The glycopeptides were then separated and analyzed by nanoLC-Chip Q-TOF MS. The LC/MS data indicate that the mutated L28N in M1 and M7 IFNλ4 variants were not glycosylated, whereas an original N-glycosylation site, Asn61, and mutated P73N were fully occupied by N-glycans (Fig. 3B–D). These are in accordance with the PNGase F treatment results, where M1 (L28N) migrated more quickly than either M3 (P73N) or M7 (L28N + P73N).

3.3. Receptor binding affinity and biological activity of IFNλ4 variants

To investigate whether the mutation and the additional glycan on IFNλ4 variants affect their binding to their receptors, IL10Rβ and IFNλR1, we examined the *in vitro* binding affinity of IFNλ4 variants to IL10Rβ and IFNλR1 by Biolayer Light Interferometry (BLI) and then compared them with that of IFNλ4 WT purified from *E. coli* (eIFNλ4). Similar to eIFNλ4, the three IFNλ4 variants properly bound to their

receptors and their binding affinities to IFNλR1 were higher than to IL10Rβ (Fig. 4). Moreover, our variants had a slightly higher affinity towards IL10Rβ than the eIFNλ4 does (For IL10Rβ, $K_{D\ M1}$ = 49 nM, $K_{D\ M3}$ = 51 nM, $K_{D\ M7}$ = 49 nM, $K_{D\ eIFN\lambda4}$ = 71 nM), while their binding affinity to IFNλR1 was similar to each other (For IFNλR1, $K_{D\ M1}$ = 14 nM, $K_{D\ M3}$ = 22 nM, $K_{D\ M7}$ = 17 nM, $K_{D\ eIFN\lambda4}$ = 19 nM). The modifications elicited by mutation and glycosylation does not inhibit their interaction with their specific receptors, even further stabilize the interaction between IFNλ4 and IL10Rβ.

In order to determine whether the mutation and additional glycan

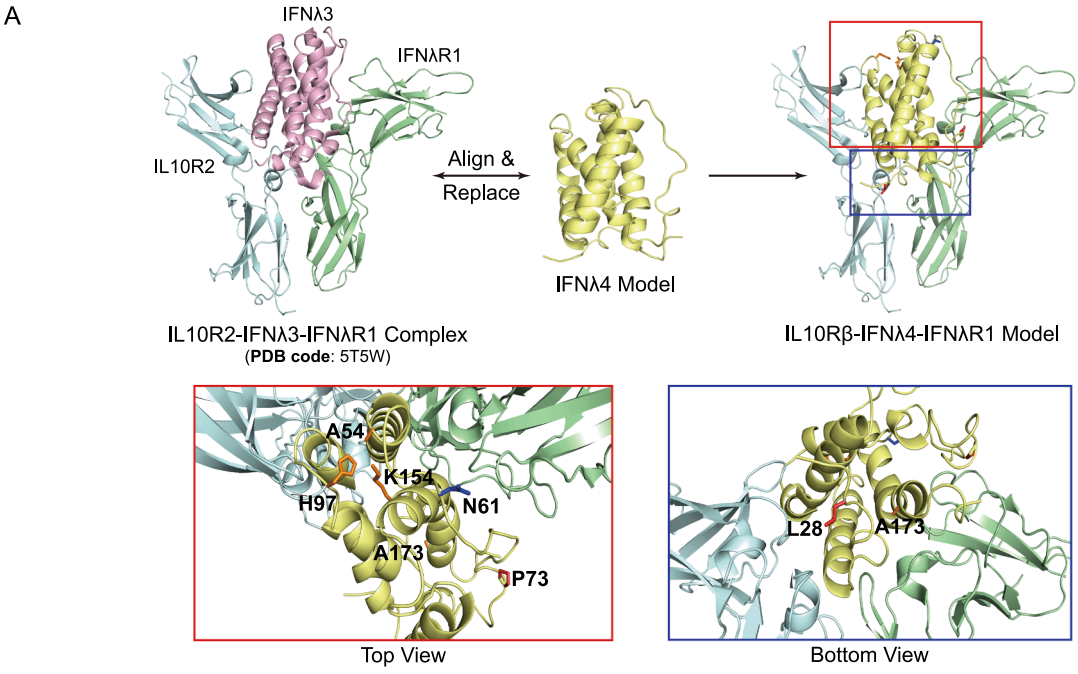

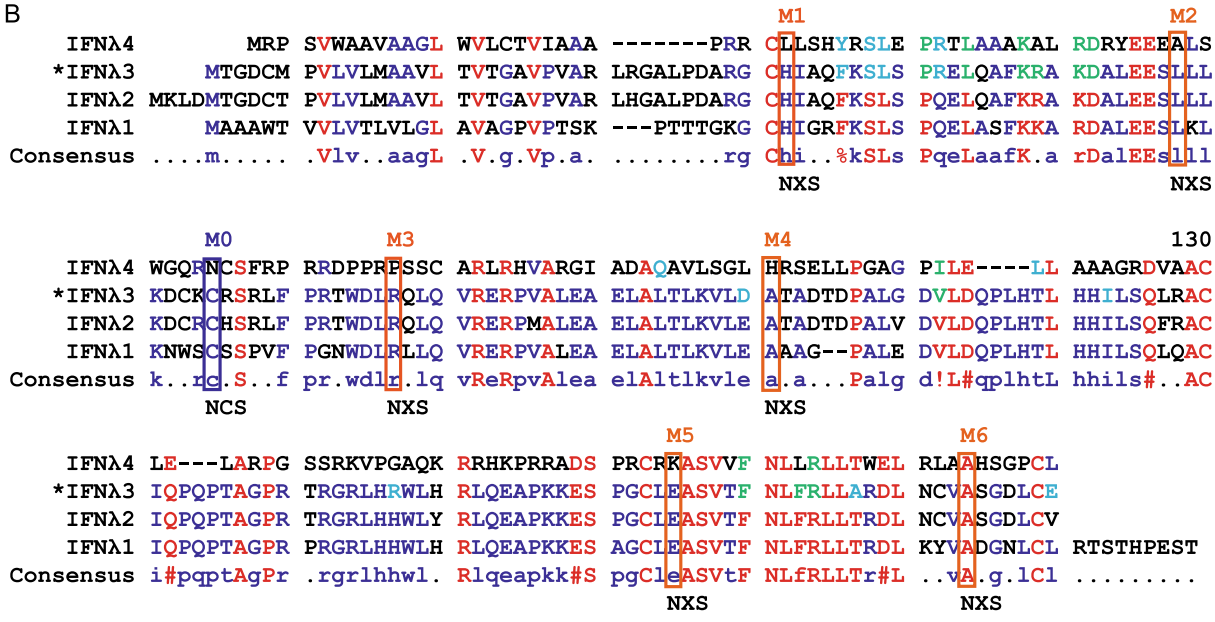

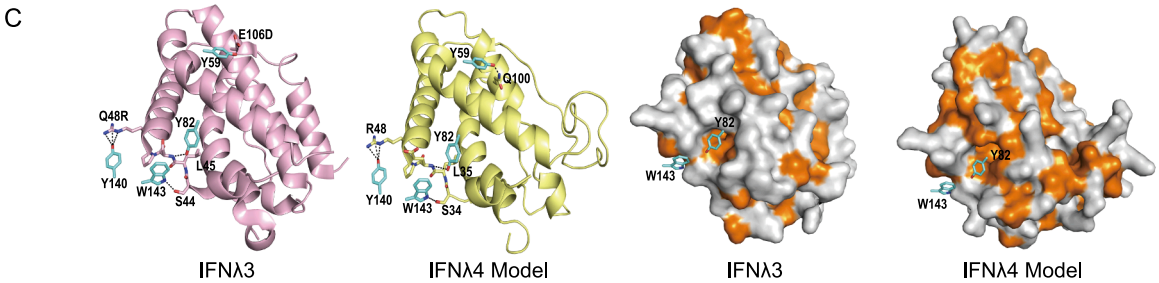

(caption on next page)

Fig. 1. Design of IFNλ4 variants. (A) Model structure of IL10Rβ-IFNλ4-IFNλR1 (right) built from the IL10Rβ-IFNλ3-IFNλR1 complex structure (PDB code: 5T5W, Left). Mutation sites for potential N-glycosylation are displayed as the orange stick model (L28, A54, P73, H97, K154, A173) and seen in two different views (bottom). The endogenous N-glycosylation site – N61 – is shown as the blue stick. (B) Sequence alignment of IFNλ proteins. Amino acids important in binding with IFNλR1 and IL10Rβ are highlighted in green and cyan, respectively. Mutation sites for potential N-glycosylation are labeled from M1 to M6 and are boxed in orange. The endogenous N-glycosylation site for IFNλ4 (N61, M0) is boxed in blue. Sequence conservation from the highest to lowest order is colored in red, blue, and black. The *IFNλ3 sequence was obtained from the crystal structure of the IL10Rβ-IFNλ3-IFNλR1 complex [23], which contains affinity-enhancing mutations on IFNλ3 for stabilizing its interaction with IL10Rβ. (C) Binding mode of IFNλ3 and IFNλ4 towards IL10Rβ. The hydrogen bond network between IFNλ3 and IL10Rβ is shown and similar interactions between IFNλ4 and IL10Rβ are mapped based on the model structure of IL10Rβ-IFNλ4-IFNλR1 (left). Surface representation of binding sites for IL10Rβ Y82 and W143 within IFNλ3 [23] and IFNλ4 (right). Hydrophobic residues are colored in orange and grey. Hydrophobic pockets for harboring the hydrophobic residues of IL10Rβ (Y82, W143) were found within both IFNλ3 and IFNλ4. (For interpretation of the references to colour in this figure legend, the reader is referred to the web version of this article.)

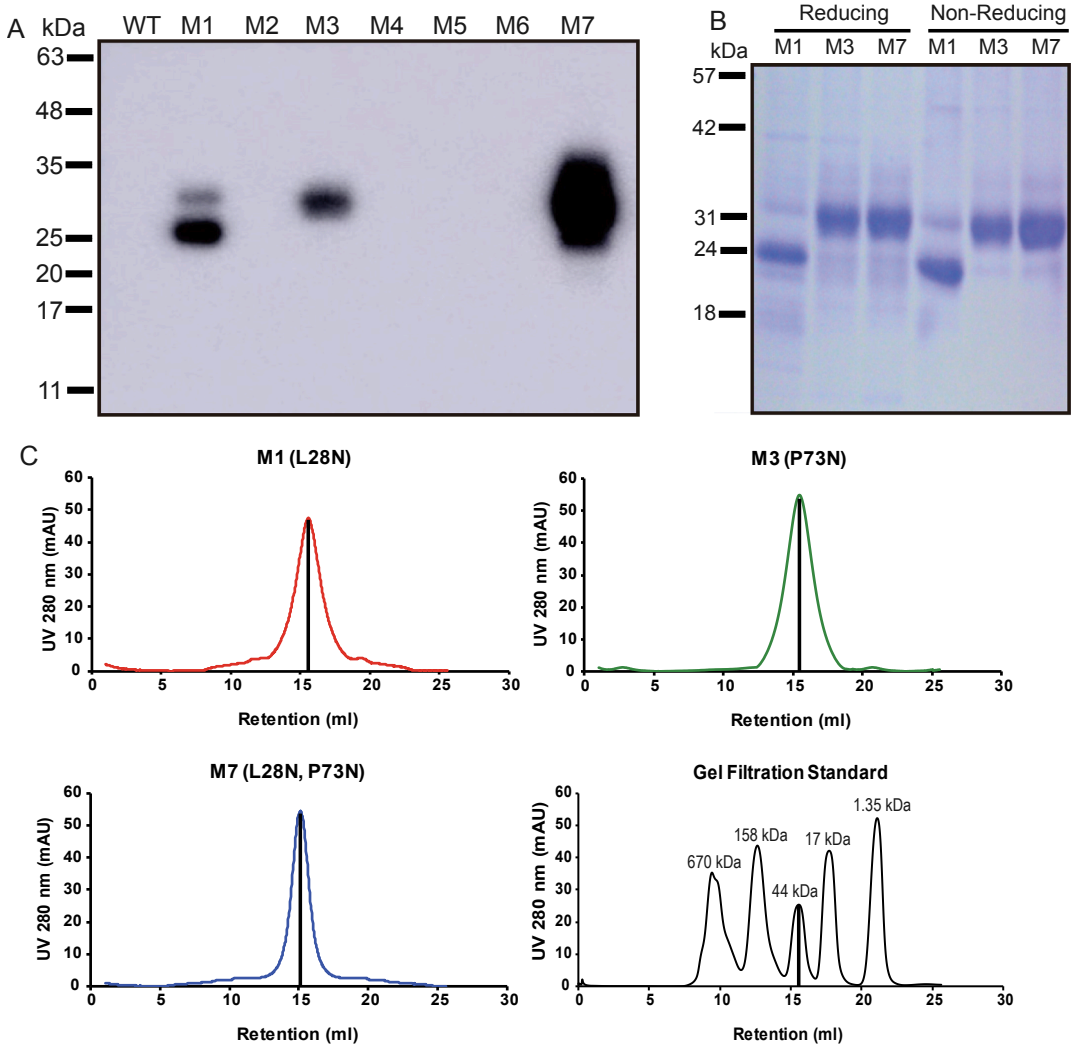

Fig. 2. Production of IFNλ4 variants. (A) Expression test of IFNλ4 variants. Expression level of IFNλ4 wild-type and variants containing C-terminal 6x-histidine tags were monitored by Western blot with anti-his antibody. M1 (L28N), M3 (P73N), and M7 (L28N + P73N) showed enhanced expression and were selected for larger scale expression. (B) Coomassie blue staining of purified M1, M3, and M7 under reducing and non-reducing condition. The proteins were purified by affinity chromatography with IgG sepharose followed by thrombin digestion and gel filtration chromatography. (C) Gel filtration chromatogram of M1, M3, M7, and standard proteins. Each gel filtration peak corresponds to standard proteins – thyroglobulin (670 kDa), γ-globulin (158 kDa), ovalbumin (44 kDa), myoglobin (17 kDa), and vitamin B12 (1.35 kDa). A bar connecting the maximum and the x-axis is drawn to help read the elution volume. (For interpretation of the references to colour in this figure legend, the reader is referred to the web version of this article.)

on the IFNλ4 variants affected their functional activity, we investigated their IFNλR1-dependent phospho-STAT1 signaling upon treatment with the IFNλ4 variants. Our results indicate that treatment with the M1, M3, and M7 IFNλ4 variants also induced phosphorylation of STAT1, just as in other type III interferons, IFNλ1∼3, and that the suppression of IFNλR1 expression by small interference RNA specific to the IFNλR1 gene (siIFNλR1) abolished the phosphorylation of STAT1, even after treatment with the IFNλ4 variants (Fig. 5A). IFNλ4 stimulation reportedly leads to the assembly of the ISGF3 transcription factor complex, which consists of phospho-STAT1, phospho-STAT2, and IRF9 and induces the expression of ISG15 [27], which is critical for anti-viral activity [28]. We showed that the M1, M3, and M7 IFNλ4 variants also induced the expression of ISG15 and inhibited HCV replication in HCV-infected Huh-7.5 cells (Fig. 5B and 5C). Interestingly, the M1, M3, and M7 IFNλ4 variants showed a significantly more potent ISG induction and anti-viral activity than eIFNλ4.

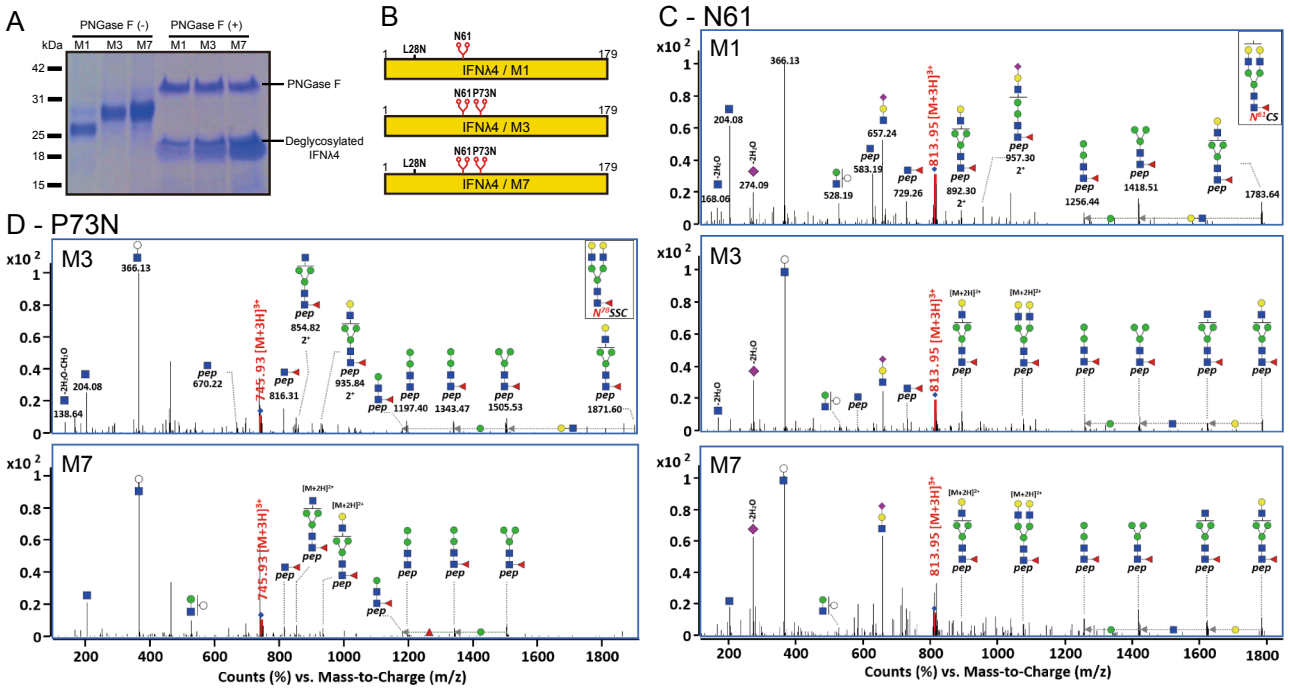

Fig. 3. Identification of N-glycosylation on IFNλ4 variants. (A) SDS-PAGE analysis with and without PNGase-F treatment of IFNλ4 variants, M1, M3, and M7. (B) Schematic diagram of IFNλ4 variants (M1, M3, M7) marked with the confirmed position of N-glycosylation by mass spectrometry. (C) Collision-induced dissociation (CID) tandem MS spectra of precursor ion at *m/z* 813.95 $[M + 3H]^{3+}$ corresponding to Hex5HexNAc4Fuc1NeuAc1 with peptide back bone (NCS) on N61 from IFNλ4 variants (M1, M3, M7). (D) CID tandem MS spectra of precursor ion at *m/z* 745.93 $[M + 3H]^{3+}$ corresponding to Hex5HexNAc4Fuc1 with peptide back bone (NSSC) on P73N from IFNλ4 variants (M3 and M7). Mutated L28Ns in M1 and M7 were not glycosylated.

Prolonged exposure to IFNλ proteins induces the production of unphosphorylated ISGF3 (U-ISGF3) consisting of STAT1, STAT2 and IRF9 without tyrosine phosphorylation while the expression of phosphorylated ISGF3 are diminished [18]. As a result, the upregulation of the U-ISGF3-specific set of genes, such as Mx1, is maintained long-term. In order to assess whether the M1, M3, and M7 variants display a similar functionality during prolonged treatment, we evaluated the protein levels of the U-ISGF3 components. The protein levels of STAT1, STAT2, and IRF9 were equally upregulated by all IFNλ4s (Fig. 5D). Nevertheless, our IFNλ4 variants maintained the upregulation of Mx1 more robustly than did eIFNλ4, but IFNλ1, 2 and 3 maintained more strongly the upregulation of Mx1 expression compared to our IFNλ4 variants (Fig. 5E).

Previously, eIFNλ4 is shown to induce the expression of negative regulators of IFN signaling [27,29] such as SOCS1 and USP18. To assess the effect of glycosylation on this functionality, we examined the expression level of SOCS1 and USP18 upon the treatment of M1, M3 and M7 variants on Huh7 cell line. USP18 was significantly increased upon treatment of IFNλ1, 2 and 3. While eIFNλ4 resulted in slight increase of USP18, our IFNλ4 variants (M1, M3 and M7) showed a comparable activity to IFNλ1, 2 and 3 (Fig. 5F). The protein expression of SOCS1 was not significantly increased by the treatment of any form of IFNλs (Fig. 5F). However, the mRNA expression of SOCS1 was slightly upregulated by IFNλs, although there was no significant difference among IFNλs (Fig. 5G). These results suggest that our structure-based approach on selecting *de novo* glycosylation maintained the biological activity of IFNλ4 and our IFNλ4 variants expressed from HEK293 have superior activity compared to eIFNλ4.

4. Discussion

Until recently, research on IFNλ4 and its use as a clinical therapeutic was hindered by the inability to obtain appreciable amounts of this protein. Purification of bacterial-derived recombinant IFNλ4 through refolding [11] still poses a number of problems, including the complexity of purification steps, lack of glycosylation, and endotoxin contamination. Our study is an example of how glycoengineering aided by structural information can be used to overcome such limitations; it is the first to report the successful production of IFNλ4 protein from a mammalian cell line with enhanced properties compared to eIFNλ4 and requiring a simpler purification protocol. There are several possibilities as to why our IFNλ4 variants displayed enhanced expression and potency. First, the presence of acidic N-glycans may stabilize the protein through a charge-balance, since IFNλ4 is unusually abundant with positively charged amino acids (~23%). Second, considering how the immune response is more actively triggered by our variants without critically affecting the receptor binding activity, compared to eIFNλ4, extra N-glycans may have extended the half-life, as in other reports [12,30], thereby increasing the fraction of functional protein during treatment. Finally, since N-glycosylation in eukaryotes is co-translational [31], the protein folding may have also been affected. Nevertheless, the mechanism behind the enhanced expression induced by unmodified L28N remains unanswered. We speculate that L28 may serve as the hydrophobic aggregation nuclei interacting with nearby hydrophobic residues, such as L29 or Y32 [32,33]; perhaps L28N alleviates this effect.

This study is unique, in that we were able to successfully identify a viable *de novo* N-glycosylation site by structural elucidation of glycopeptides. We used endogenous serine, threonine, or asparagine to introduce the glycosylation modification, which minimized the mutation-induced structural distortion. Other IFNλ4 candidates containing N-glycosylation sites at random locations were also tested (data not shown) but no additional modification or expression changes were observed, indicating the efficiency of our structure-oriented approach. However, glyco-peptides containing L28N were not detected by mass spectrometry, suggesting that the site may have remained unmodified. According to the recent cryo-EM structure of oligosaccharyltransferase (OST) [34–36], which catalyzes the initial transfer of glycan from the

A

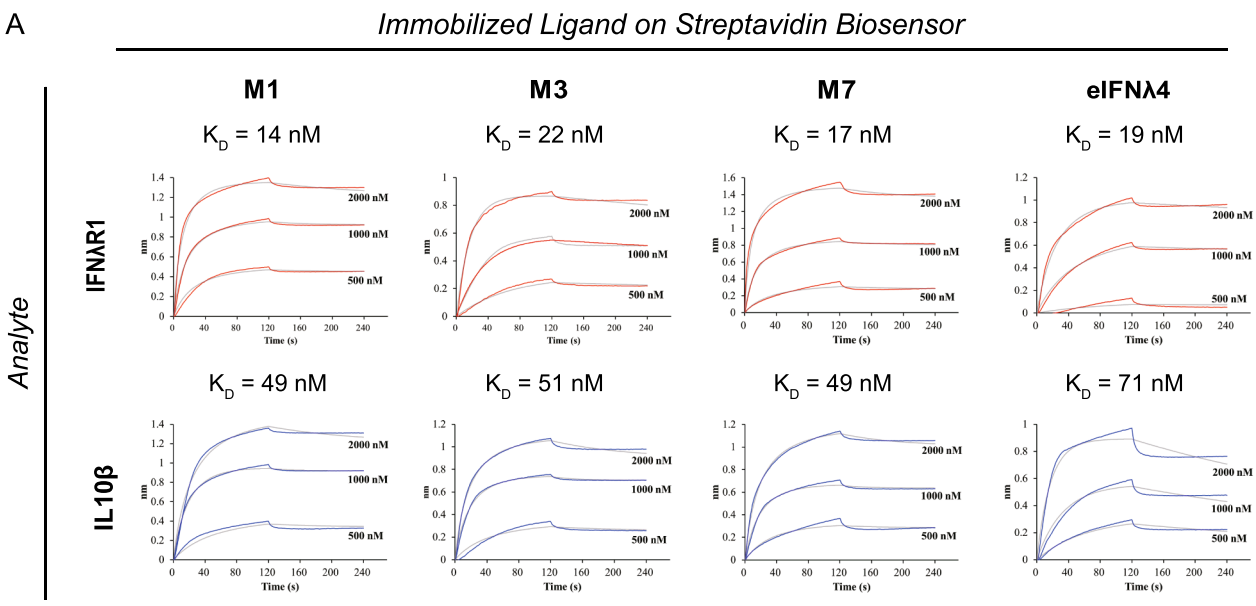

B

		K_D (nM)	k_{on} (1/Ms)	k_{dis} (1/s)	χ^2	R^2
IFNλR1	M1	14	5.02E+04	6.86E-04	0.0013	0.993
	M3	22	2.92E+04	6.47E-04	0.0012	0.9872
	M7	17	5.83E+04	9.67E-04	0.0013	0.9745
	eIFNλ4	19	2.13E+04	3.97E-04	0.0081	0.9836
IL10Rβ	M1	49	2.13E+04	1.04E-03	0.0026	0.9883
	M3	51	2.91E+04	1.48E-03	0.002	0.9911
	M7	49	2.62E+04	1.29E-03	0.0121	0.9866
	eIFNλ4	71	2.88E+04	2.03E-03	0.0027	0.9395

Fig. 4. Binding kinetics of IFNL4 variants with IFNλR1 or IL10Rβ. (A) Binding curves of IFNλR1 and IL10Rβ toward IFNλ4 variants (M1, M3, M7) and eIFNλ4 at the indicated concentrations of IFNλR1 and IL10Rβ (500, 1000, 2000 nM). Sensorgrams were obtained from BLItz instrument. Data points are shown in grey and the corresponding fits are shown in red (IFNλR1) and blue (IL10Rβ). K_D values were calculated from 1:1 global fitting. (B) Binding kinetics of IFNλR1 and IL10Rβ to immobilized IFNλ4 variants (M1, M3, M7) and eIFNλ4. Goodness of fit was assessed by evaluating the χ^2 and R^2 values generated for all fitting analyses. (For interpretation of the references to colour in this figure legend, the reader is referred to the web version of this article.)

lipid-linked oligosaccharide onto the substrate asparagine, substrate binding to the catalytic subunit, STT3, requires structural flexibility near the glycosylation sequence of the substrate. Our IFNλ4 model suggests that P73 is located on the flexible loop, while other eliminated candidate sites (A173 and K154) are part of the α-helix. This may partly explain the successful glycosylation of P73N. On the contrary, L28N may not be physically accessible by OST. Elucidating the structure of IFNλ4 may provide insights to this hypothesis.

A number of interferons are already targets of drug development, due to their ability to generate strong antiviral and antitumor responses or to modulate immune responses. IFNα and its PEGylated variants are used against cancers such as hairy cell leukemia (Roferon A), melanoma (Multiferon), and AIDS-related Kaposi's sarcoma (Intron A) [37–39]. IFNβ is a well-known treatment for multiple sclerosis, with a number of different versions available (Rebif – IFNβ 1a, liquid form, Avonex – IFNβ 1a, lyophilized, Cinnovex – IFNβ 1a, biogeneric, Betaseron – IFNβ 1b, Plegridy – PEGylated IFNβ 1a) [40–43]. Similar to this, IFNλs also have a therapeutic potential, because it has been shown that IFNλs can protect hosts from various viruses, including influenza virus, West Nile virus, norovirus and rotavirus [38–41]. It will be very interesting to test if glycosylated IFNλs exert anti-viral activity in hosts infected by such viruses. In this regard, a recent study demonstrated that IFNλs can suppress influenza virus without the inflammatory side effects of IFNα [44]. However, it was previously shown that the expression of functional IFNλ4 is associated with unresponsiveness to IFNα treatment among HCV-infected patients [9], and a subsequent study showed that long-term exposure to IFNλ4 leads to cellular unresponsiveness to IFNα treatment by upregulation of USP18 or SOCS1 [27,29], indicating that IFNλ4 treatment may be detrimental to virus-infected patients. On the other hand, our result shown in Fig. 5C indicates that IFNλ4 treatment can directly suppress HCV replication. Whether IFNλ4 treatment will be beneficial or detrimental to virus-infected patients might be determined by duration of the treatment and use of IFNα following IFNλ4 treatment. Although much further research and insight into the mode of action of IFNλ4 is required to understand if its effects are beneficial or detrimental to human health, our engineered IFNλ4 variants can be utilized as an alternative platform of IFNλ4 wild-type.

Declaration of Competing Interest

The authors declare that they have no known competing financial interests or personal relationships that could have appeared to

influence the work reported in this paper.

Acknowledgments

This work was supported by the National Research Foundation of Korea (NRF) grant (2015M3A9B5053960 to H.M.K. and H.J.A) and the Korean Health Technology R&D Project, Ministry of Health and Welfare (HI18C0135 to H.M.K.).

Author contributions

J.H.C., S.H.H., H.J.A, E.C.S., and H.M.K. designed the experiments; J.H.C., S.H.H., and N.S. contributed to the experimental work; J.H.C., P.L., E.C.S., and H.M.K. wrote and edited the manuscript. E.C.S. and

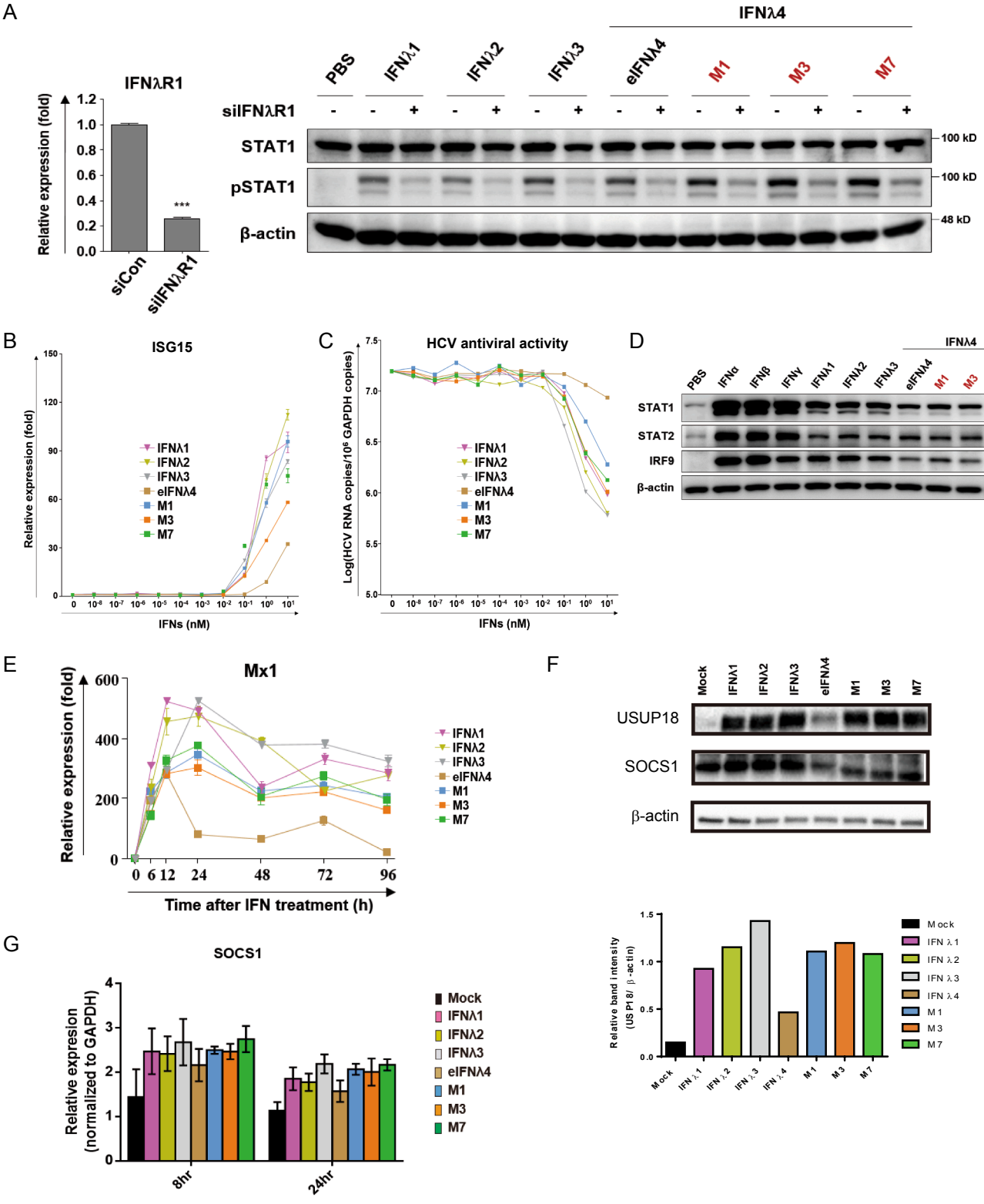

(caption on next page)

Fig. 5. Biological activity of IFNλ4 variants. (A) Activation of the JAK-STAT pathway by IFNλ4 variants via the IFNλ receptor. Huh-7.5 cells were treated with IFNλs or IFNλ4 variants (10 nM) for 30 min. The expression of IFNλR1 was suppressed by IFNλR1-specific siRNA (siIFNλR1) to show changes in the phosphorylation level of STAT1 (pSTAT1) triggered by IFNλ4 variants (eIFNλ4, M1, M3, and M7 IFNλ4 variants). (B) Induction of interferon-stimulated gene 15 (ISG15) expression by IFNλ4 variants in Huh-7.5 cells. Huh-7.5 cells were treated with 10 nM IFNλs for 10 h. (C) Inhibition of HCV replication by IFNλ4 variants. HCVcc-infected Huh-7.5 cells were treated with the indicated concentration of IFNλs for 48 h. (D) Production of U-ISGF3 by the prolonged treatment of IFNλ4 variants. Huh-7.5 cells were treated with 10 nM IFNα, IFNβ, IFNγ, or IFNλs for 72 h. Extended exposure to type III interferons induced the expression of U-ISGF3, which was composed of IRF9, unphosphorylated STAT1, and unphosphorylated STAT2. Similar responses by IFNλ4 variants were monitored. (E) Upregulation of Mx1 after prolonged treatment with IFNλs (10 nM). Mx1 is preferentially expressed by U-ISGF3 after prolonged treatment with type III interferons. (F) Immunoblotting of USP18 and SOCS1 at 48 h after treating IFNλs with final concentration of 10 nM on Huh7.5 cells. Band intensity of USP18 versus β-actin is shown below the blot image. (G) Induction of SOCS1 expression by 10 nM IFNλs treatment in Huh-7.5 cells. Relative expression was determined at 8- and 24-hour post-treatment by real-time quantitative PCR. In (A), (D) and (F), immunoblots are representative of three independent experiments with similar results. In (B), (C), (E), and (G), all analyses were done with triplicates and the graphs are representative of three independent experiments with similar results.

H.M.K. supervised the project. All authors reviewed the manuscript.

Appendix A. Supplementary material

Supplementary data to this article can be found online at https://doi.org/10.1016/j.cyto.2019.154833.

References

[1] L.C. Platanias, Mechanisms of type-I- and type-II-interferon-mediated signalling, Nat. Rev. Immunol. 5 (2005) 375–386.
[2] F. McNab, K. Mayer-Barber, A. Sher, A. Wack, A. O'Garra, Type I interferons in infectious disease, Nat. Rev. Immunol. 15 (2015) 87–103.
[3] A. Wack, E. Terczynska-Dyla, R. Hartmann, Guarding the frontiers: the biology of type III interferons, Nat Immunol 16 (2015) 802–809.
[4] S.V. Kotenko, J.E. Durbin, Contribution of type III interferons to antiviral immunity: location, location, location, J. Biol. Chem. 292 (2017) 7295–7303.
[5] A. Lasfar, A. Zloza, K.A. Cohen-Solal, IFN-lambda therapy: current status and future perspectives, Drug Discovery Today 21 (2016) 167–171.
[6] E. Andreakos, I. Zanoni, I.E. Galani, Lambda interferons come to light: dual function cytokines mediating antiviral immunity and damage control, Curr. Opin. Immunol. 56 (2019) 67–75.
[7] S.V. Kotenko, G. Gallagher, V.V. Baurin, A. Lewis-Antes, M. Shen, N.K. Shah, et al., IFN-lambdas mediate antiviral protection through a distinct class II cytokine receptor complex, Nat. Immunol. 4 (2003) 69–77.
[8] P. Sheppard, W. Kindsvogel, W. Xu, K. Henderson, S. Schlutsmeyer, T.E. Whitmore, et al., IL-28, IL-29 and their class II cytokine receptor IL-28R, Nat. Immunol. 4 (2003) 63–68.
[9] L. Prokunina-Olsson, B. Muchmore, W. Tang, R.M. Pfeiffer, H. Park, H. Dickensheets, et al., A variant upstream of IFNL3 (IL28B) creating a new interferon gene IFNL4 is associated with impaired clearance of hepatitis C virus, Nat. Genet. 45 (2013) 164–171.
[10] E. Terczynska-Dyla, S. Bibert, F.H. Duong, I. Krol, S. Jorgensen, E. Collinet, et al., Reduced IFNlambda4 activity is associated with improved HCV clearance and reduced expression of interferon-stimulated genes, Nat. Commun. 5 (2014) 5699.
[11] O.J. Hamming, E. Terczynska-Dyla, G. Vieyres, R. Dijkman, S.E. Jorgensen, H. Akhtar, et al., Interferon lambda 4 signals via the IFNlambda receptor to regulate antiviral activity against HCV and coronaviruses, EMBO J. 32 (2013) 3055–3065.
[12] K. Song, I.S. Yoon, N.A. Kim, D.H. Kim, J. Lee, H.J. Lee, et al., Glycoengineering of interferon-beta 1a improves its biophysical and pharmacokinetic properties, PLoS ONE 9 (2014) e96967.
[13] N. Ceaglio, M. Etcheverrigaray, R. Kratje, M. Oggero, Novel long-lasting interferon alpha derivatives designed by glycoengineering, Biochimie 90 (2008) 437–449.
[14] C.M. Sagt, B. Kleizen, R. Verwaal, M.D. de Jong, W.H. Muller, A. Smits, et al., Introduction of an N-glycosylation site increases secretion of heterologous proteins in yeasts, Appl. Environ. Microbiol. 66 (2000) 4940–4944.
[15] Y. Liu, A. Nguyen, R.L. Wolfert, S. Zhuo, Enhancing the secretion of recombinant proteins by engineering N-glycosylation sites, Biotechnol. Prog. 25 (2009) 1468–1475.
[16] S. Hua, C.Y. Hu, B.J. Kim, S.M. Totten, M.J. Oh, N. Yun, et al., Glyco-analytical multispecific proteolysis (Glyco-AMP): a simple method for detailed and quantitative Glycoproteomic characterization, J. Proteome Res. 12 (2013) 4414–4423.
[17] H.J. An, J.S. Tillinghast, D.L. Woodruff, D.M. Rocke, C.B. Lebrilla, A new computer program (GlycoX) to determine simultaneously the glycosylation sites and oligosaccharide heterogeneity of glycoproteins, J. Proteome Res. 5 (2006) 2800–2808.
[18] P.S. Sung, H. Cheon, C.H. Cho, S.H. Hong, D.Y. Park, H.I. Seo, et al., Roles of unphosphorylated ISGF3 in HCV infection and interferon responsiveness, Proc. Natl. Acad. Sci. U S A 112 (2015) 10443–10448.
[19] W. Kang, E.C. Shin, Colorimetric focus-forming assay with automated focus counting by image analysis for quantification of infectious hepatitis C virions, PLoS ONE 7 (2012) e43960.
[20] P.S. Sung, A. Murayama, W. Kang, M.S. Kim, S.K. Yoon, M. Fukasawa, et al., Hepatitis C virus entry is impaired by claudin-1 downregulation in diacylglycerol acyltransferase-1-deficient cells, J. Virol. 88 (2014) 9233–9244.
[21] H.H. Gad, C. Dellgren, O.J. Hamming, S. Vends, S.R. Paludan, R. Hartmann, Interferon-lambda is functionally an interferon but structurally related to the interleukin-10 family, J. Biol. Chem. 284 (2009) 20869–20875.
[22] Z.J. Miknis, E. Magracheva, W. Li, A. Zdanov, S.V. Kotenko, A. Wlodawer, Crystal structure of human interferon-lambda1 in complex with its high-affinity receptor interferon-lambdaR1, J. Mol. Biol. 404 (2010) 650–664.
[23] J.L. Mendoza, W.M. Schneider, H.H. Hoffmann, K. Vercauteren, K.M. Jude, A. Xiong, et al., The IFN-lambda-IFN-lambdaR1-IL-10Rbeta Complex Reveals Structural Features Underlying Type III IFN Functional Plasticity, Immunity 46 (2017) 379–392.
[24] M. Chavan, W. Lennarz, The molecular basis of coupling of translocation and N-glycosylation, Trends Biochem. Sci. 31 (2006) 17–20.
[25] R. Kornfeld, S. Kornfeld, Assembly of asparagine-linked oligosaccharides, Annu. Rev. Biochem. 54 (1985) 631–664.
[26] M.J. Oh, S. Hua, U. Kim, H.J. Kim, J. Lee, J.H. Kim, et al., Analytical detection and characterization of biopharmaceutical glycosylation by MS, Bioanalysis 8 (2016) 711–727.
[27] P.S. Sung, S.H. Hong, J.H. Chung, S. Kim, S.H. Park, H.M. Kim, et al., IFN-lambda4 potently blocks IFN-alpha signalling by ISG15 and USP18 in hepatitis C virus infection, Sci. Rep. 7 (2017) 3821.
[28] J.W. Schoggins, C.M. Rice, Interferon-stimulated genes and their antiviral effector functions, Curr. Opin. Virol. 1 (2011) 519–525.
[29] A.A. Obajemu, N. Rao, K.A. Dilley, J.M. Vargas, F. Sheikh, R.P. Donnelly, et al., IFN-lambda4 attenuates antiviral responses by enhancing negative regulation of IFN signaling, J. Immunol. 199 (2017) 3808–3820.
[30] A.M. Sinclair, S. Elliott, Glycoengineering: the effect of glycosylation on the properties of therapeutic proteins, J. Pharm. Sci. 94 (2005) 1626–1635.
[31] D.J. Kelleher, R. Gilmore, An evolving view of the eukaryotic oligosaccharyltransferase, Glycobiology 16 (2006) 47R–62R.
[32] N. Chennamsetty, V. Voynov, V. Kayser, B. Helk, B.L. Trout, Design of therapeutic proteins with enhanced stability, Proc. Natl. Acad. Sci. U S A 106 (2009) 11937–11942.
[33] C.J. Roberts, Therapeutic protein aggregation: mechanisms, design, and control, Trends Biotechnol. 32 (2014) 372–380.
[34] L. Bai, T. Wang, G. Zhao, A. Kovach, H. Li, The atomic structure of a eukaryotic oligosaccharyltransferase complex, Nature 555 (2018) 328–333.
[35] K. Braunger, S. Pfeffer, S. Shrimal, R. Gilmore, O. Berninghausen, E.C. Mandon, et al., Structural basis for coupling protein transport and N-glycosylation at the mammalian endoplasmic reticulum, Science 360 (2018) 215–219.
[36] R. Wild, J. Kowal, J. Eyring, E.M. Ngwa, M. Aebi, K.P. Locher, Structure of the yeast oligosaccharyltransferase complex gives insight into eukaryotic N-glycosylation, Science 359 (2018) 545–550.
[37] J.R. Quesada, E.M. Hersh, J. Manning, J. Reuben, M. Keating, E. Schnipper, et al., Treatment of hairy cell leukemia with recombinant alpha-interferon, Blood 68 (1986) 493–497.
[38] R. Stadler, T. Luger, T. Bieber, U. Kohler, R. Linse, K. Technau, et al., Long-term survival benefit after adjuvant treatment of cutaneous melanoma with dacarbazine and low dose natural interferon alpha: A controlled, randomised multicentre trial, Acta Oncol. 45 (2006) 389–399.
[39] P.A. Volberding, R.T. Mitsuyasu, J.P. Golando, R.J. Spiegel, Treatment of Kaposi's sarcoma with interferon alfa-2b (Intron A), Cancer 59 (1987) 620–625.
[40] M. Mazdeh, S. Afzali, M.R. Jaafari, The therapeutic effect of Avonex, Rebif and Betaferon on EDSS and relapse in multiple sclerosis: a comparative study, Acta Medica Iranica 48 (2010) 83–88.
[41] M. Sanford, K.A. Lyseng-Williamson, Subcutaneous recombinant interferon-beta-1a (Rebif(R)): a review of its use in the treatment of relapsing multiple sclerosis, Drugs 71 (2011) 1865–1891.
[42] H. Pakdaman, M. Abbasi, K. Gharagozli, F. Ashrafi, H. Delavar Kasmaei, Harandi A. Amini, A randomized double-blind trial of comparative efficacy and safety of Avonex and CinnoVex for treatment of relapsing-remitting multiple sclerosis, Neurol. Sci.: Official J. Italian Neurol. Soc. Italian Soc. Clin. Neurophysiol. 39 (2018) 2107–2113.
[43] Peginterferon beta-1a (Plegridy) for multiple sclerosis. The Medical letter on drugs and therapeutics 2015; 57: pp. 67–9.
[44] S. Davidson, T.M. McCabe, S. Crotta, H.H. Gad, E.M. Hessel, S. Beinke, et al., IFNlambda is a potent anti-influenza therapeutic without the inflammatory side effects of IFNalpha treatment, EMBO Mol. Med. 8 (2016) 1099–1112.